

Half-metallic ferromagnetic Weyl fermions related to dynamic correlations in the zinc-blende compound VAs

Xianyong Ding(丁献勇), Haoran Wei(魏皓然), Ruixiang Zhu(朱瑞翔), Xiaoliang Xiao(肖晓亮), Xiaozhi Wu(吴小志), and Rui Wang(王锐)

Citation: Chin. Phys. B, 2024, 33 (**9**): 097103. DOI: 10.1088/1674-1056/ad5f86
Journal homepage: http://cpb.iphy.ac.cn; http://iopscience.iop.org/cpb

What follows is a list of articles you may be interested in

Coexistence of Dirac and Weyl points in non-centrosymmetric semimetal $NbIrTe_4$

Qingxin Liu(刘清馨), Yang Fu(付阳), Pengfei Ding(丁鹏飞), Huan Ma(马欢), Pengjie Guo(郭朋杰), Hechang Lei(雷和畅), and Shancai Wang(王善才)
Chin. Phys. B, 2024, 33 (**4**): 047104. DOI: 10.1088/1674-1056/ad2a79

Angle-resolved photoemission study of NbGeSb with non-symmorphic symmetry

Huan Ma(马欢), Ning Tan(谭宁), Xuchuan Wu(吴徐传), Man Li(李满), Yiyan Wang(王义炎), Hongyan Lu(路洪艳), Tianlong Xia(夏天龙), and Shancai Wang(王善才)
Chin. Phys. B, 2024, 33 (**2**): 027102. DOI: 10.1088/1674-1056/ad0ccf

Electronic structure of cuprate-nickelate infinite-layer heterostructure

Dachuan Chen(陈大川), Paul Worm, Liang Si(司良), Chunxiao Zhang(张春小), Fenglin Deng(邓凤麟), Peiheng Jiang(蒋沛恒), and Zhicheng Zhong(钟志诚)
Chin. Phys. B, 2023, 32 (**8**): 087105. DOI: 10.1088/1674-1056/acd368

Thermal spin molecular logic gates modulated by an electric field

Xingyi Tan(谭兴毅), Qiang Li(李强), and Dahua Ren(任达华)
Chin. Phys. B, 2023, 32 (**5**): 057101. DOI: 10.1088/1674-1056/ac89e5

Predicting novel atomic structure of the lowest-energy Fe_nP_{13-n} (n=0-13) clusters: A new parameter for characterizing chemical stability

Yuanqi Jiang(蒋元祺) and Ping Peng(彭平)
Chin. Phys. B, 2023, 32 (**4**): 047102. DOI: 10.1088/1674-1056/acae75

Half-metallic ferromagnetic Weyl fermions related to dynamic correlations in the zinc-blende compound VAs

Xianyong Ding(丁献勇)[1,2], Haoran Wei(魏皓然)[1,2], Ruixiang Zhu(朱瑞翔)[1,2], Xiaoliang Xiao(肖晓亮)[1,2], Xiaozhi Wu(吴小志)[1,2], and Rui Wang(王锐)[1,2,†]

[1] *Institute for Structure and Function & Department of Physics & Chongqing Key Laboratory for Strongly Coupled Physics, Chongqing University, Chongqing* 400044, *China*

[2] *Center of Quantum Materials and Devices, Chongqing University, Chongqing* 400044, *China*

(Received 15 May 2024; revised manuscript received 3 July 2024; accepted manuscript online 5 July 2024)

The realization of 100% polarized topological Weyl fermions in half-metallic ferromagnets is of particular importance for fundamental research and spintronic applications. Here, we theoretically investigate the electronic and topological properties of the zinc-blende compound VAs, which was deemed as a half-metallic ferromagnet related to dynamic correlations. Based on the combination of density functional theory and dynamical mean field theory, we uncover that the half-metallic ferromagnet VAs exhibits attractive Weyl semimetallic behaviors which are very close to the Fermi level in the DFT + U regime with effect U values ranging from 1.5 eV to 2.5 eV. Meanwhile, we also investigate the magnetization-dependent topological properties; the results show that the change of magnetization directions only slightly affects the positions of Weyl points, which is attributed to the weak spin–orbital coupling effects. The topological surface states of VAs projected on semi-infinite (001) and (111) surfaces are investigated. The Fermi arcs of all Weyl points are clearly visible on the projected Fermi surfaces. Our findings suggest that VAs is a fully spin-polarized Weyl semimetal with many-body correlated effects in the effective U values range from 1.5 eV to 2.5 eV.

Keywords: density functional theory, Weyl semimetal, dynamical mean field theory, half metallic ferromagnet

PACS: 71.55.Ak, 71.15.Dx, 75.50.Gg **DOI:** 10.1088/1674-1056/ad5f86

Half metallic ferromagnets (HMFs), which are metals for one spin polarization and semiconductors for the other, were first reported in XMnSb (X = Ni, Pt) by Groot *et al.*[1–3] HMFs that show the behaviors of a full spin-polarization of carriers are necessary to boost the efficiency of spintronic devices.[4] It is also vital for fundamental research, particularly for the origin of half-metallic gaps, nature of interatomic exchange interactions,[5] or effects of electronic correlations.[6] Due to their potential applications in spintronics and abundant correlation physics, the HMFs have attracted intensive attention and growing interest.[6–8] In recent decades, such electronic features are found in many magnetic materials, including perovskite structures,[9] CrO_2,[10] Fe_3O_4,[11] Heusler alloys,[12–19] diluted magnetic semiconductors,[20,21] spin gapless semiconductors,[22,23] topological semimetals (TSMs),[24,25] etc.

In binary transition metal compounds, two-dimensional (2D) XY (X = V, Cr; Y = P, As) and three-dimensional (3D) systems of MnAs, CrAs, and MnC were found to be HMF materials.[26–31] The zinc-blende compounds of transition elements V, Cr, and Mn with sp elements N, P, As, Sb, S, Se, and Te were reported to exhibit 100% spin polarization and half-metallic behaviors; and especially, the zinc-blende compounds VAs, VSb, CrAs, CrSb, VTe, CrSe, and CrTe were suggested to be promising candidate materials.[32] Among these compounds, CrAs has been successfully synthesized and confirmed to possess half-metallic properties both by experiments and first-principles calculations.[33–35] Another important compound in this family of materials is VAs, which was reported to be a ferromagnetic semiconductor with high Curie temperature[32,36] using density functional theory (DFT) calculations but a half-metallic ferromagnetic state using DFT plus dynamical mean field theory (DFT + DMFT) approach.[37]

On the other hand, a closing of band gap induced by dynamical correlations in VAs would potentially accompany with topological transitions. Weyl semimetals (WSMs)[38,39] are widely studied theoretically and experimentally.[40–43] Most theoretical efforts for predicting WSMs are supported by first-principles calculations within the DFT framework.[38,44–46] The HMFs may be in the case of strongly correlated electron systems. For such systems, promising topological states related promising topological states would be present. Considering that the zinc-blende VAs lacks spatial inversion symmetry and time-reversal symmetry, half-metallic ferromagnetic Weyl fermions with the dynamical many-electron feature are expected.

In this work, we delve into the correlation effects within the zinc-blende compound VAs, employing a combination of DFT and dynamical mean field theory (DMFT). Initially, we compute the electronic properties of VAs using the DFT + DMFT method in the absence of spin–orbit coupling; the

†Corresponding author. E-mail: rcwang@cqu.edu.cn

© 2024 Chinese Physical Society and IOP Publishing Ltd

methodology has been validated in numerous strong correlation systems. With DFT + DMFT serving as the benchmark, we investigate the electronic properties of VAs by systematically adjusting the effective U values, ranging from 0 eV to 4 eV. Considering that the electronic behaviors of VAs align more closely with those obtained from DFT + DMFT when the effective U values (U_{eff}) fall within the range of 0 eV–2.5 eV, we systematically explore the corresponding results using these distinct U_{eff} values under the framework of the DFT + U methods. In the U_{eff} range of 0 eV–1.0 eV, VAs exhibits trivial magnetic half-metal properties. However, within the 1.5 eV–2.5 eV interval, VAs displays noteworthy Weyl semimetal characteristics. The magnetic anisotropy energy indicates a pronounced preference for the magnetic orientation along the [001] direction with the computed magnetic moment being $2\mu_{\text{B}}$ for each V atom per unit formula. The topological surface states and Fermi arcs of (001) and (111) surfaces of VAs can be clearly visible in different energies with many Weyl points (WPs) in the entire Brillouin zone. The WPs are closed to the Fermi level and distributed asymmetrically in the first Brillouin zone due to the absence of time-reversal and inversion symmetries. In addition, the highest energy of magnetic order along [111] direction is also investigated and shows Weyl semimetal properties when $U_{\text{eff}} = 1.5$ eV. Moreover, the DFT + DMFT band structure also shows band-crossing features around these Weyl points, confirming the existence of Weyl semimetal properties. The combination of DFT + DMFT and DFT + U suggests that VAs possesses Weyl semimetal properties and will be used for spintronic applications.

As depicted in Fig. 1(a), VAs crystallizes in an FCC lattice with a space group of $F\bar{4}3m$ (No. 216). The lattice parameters are optimized to 5.74 Å with $U_{\text{eff}} = 1.5$ eV which is consistent with the values of the previous result.[37] The absence of negative phonon energies in Fig. 1(c) confirms the dynamical stability of the zinc-blende VAs compound. Figure 1(b) illustrates the three-dimensional Brillouin zone (BZ), high-symmetry points, and the corresponding surface BZ of (001) and (111) surfaces for VAs compound, which will be used in the following calculations. The fitting precision in Fig. 1(d) is obtained by using the maximal localized wannier functions (MLWFs) in the absence of the spin–orbital coupling (SOC) effect. The Wannier subspace composed by these MLWFs will be used in the following dynamical mean field calculations.

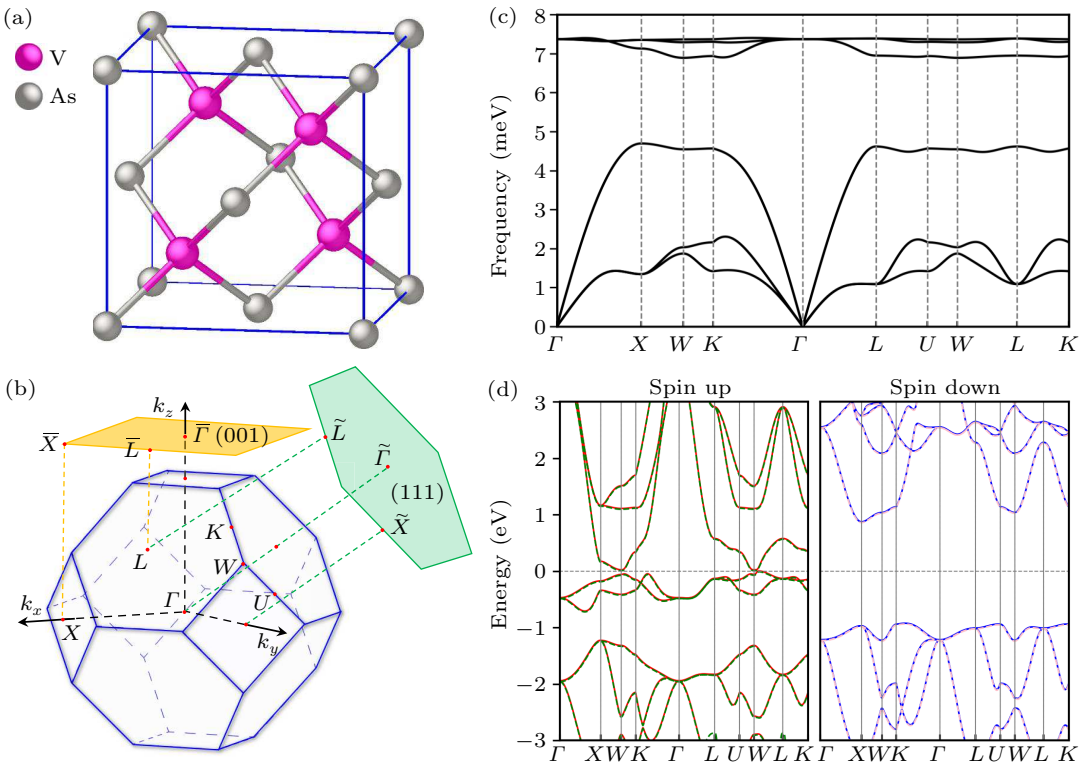


Fig. 1. (a) Crystal structure of the unit cell for VAs with space group of $F\bar{4}3m$ (No. 216), in which the red ball represents V element and gray ball represents As element. (b) The first BZ of VAs, the yellow and green color planes represent the (001) and (111) surface BZ. (c) Phonon spectrum of VAs. (d) The spin-polarized band structures of VAs. The red and blue solid lines denote different spin components computed with PBE functionals, and the green and pink dotted lines represent the corresponding results constructed with MLWFs.

It is reported in previous work[37] that zinc-blende compound VAs is a narrow band gap semiconductor by considering the correlation effect through density functional theory LSDA + U ($U = 2.0$ eV, $J = 0.9$ eV) method for V-d orbital. However, it shows metallic behavior when treating the correlation effect in the framework of DFT + DMFT. These results reveal that the electronic properties of VAs can not be determined only by using the DFT method. Here, we define

V-3d orbitals as the correlation subspace to solve the DMFT equations. As displayed in Fig. 1(d), the MLWFs of V-3d and As-4p are constructed by using Wannier90[47,48] code over the energy range $[-5.0, 4.7]$ eV concerning the Fermi energy. The hybridization window is spanned by the p–d manifold, in which V-3d orbitals are treated as the correlated orbitals. Then, DFT + DMFT calculations are implemented with the correlated subspace in which the Hubbard interaction strength $U = 5$ eV and the Hund's interaction strength $J = 1$ eV are used. The parameters for double-counting of U as $U - \alpha$ are set to DC_type $= 1$ and $\alpha = 0.2$. The different DC types are tested for minor effects on the band structure of VAs in Fig. S1 of the supplementary material (SM).[49] The DMFT impurity problem is solved using the continuous-time quantum Monte Carlo (CTQMC)[50,51] method with a temperature of 300 K and we also display the result at the temperature 200 K in Fig. S1(c). It is found that the band structure around the Fermi level remains unaffected by temperatures. Therefore, we primarily focus on the results at room temperature.

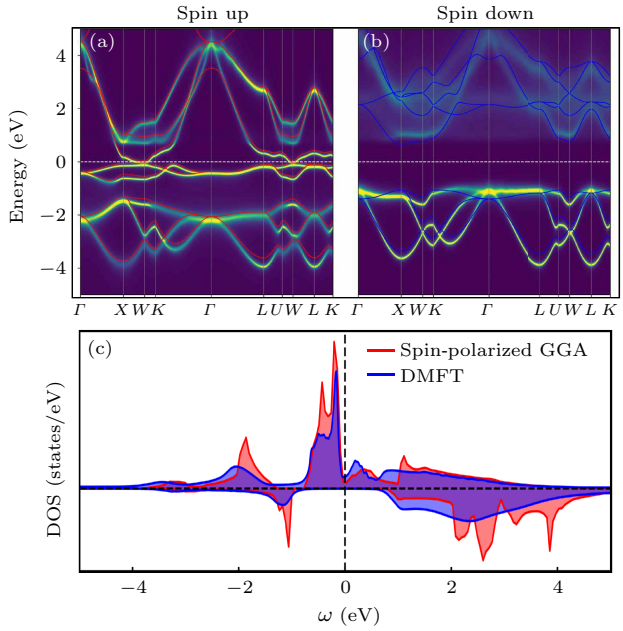


Fig. 2. [(a) and (b)] Band structure of VAs calculated by DFT + DMFT approach at the temperature of 300 K and DFT + U method without considering SOC effect, in which the left panel represents spin-up components and the right panel represents spin-down components of VAs with V sublattice forming ferromagnetic order. (c) The density of states of V-d orbitals obtained from DFT + DMFT and DFT + U methods.

Figures 2(a) and 2(b) depict the electronic structures of VAs obtained through DFT + DMFT and DFT + U methodologies, respectively, without considering the SOC effect. The combination of DFT and DMFT suggests that VAs shows half-metal properties that are consistent with the literature,[37] and the total density of states (TDOS) summed by V-d orbitals and As-p orbitals in Fig. S2 is also consistent with previous results.[37] We also compute the density of states in different effective U values ranging from 0 eV to 4.0 eV and find that VAs exhibits semiconductor properties when $U_{\text{eff}} \geq 3.0$ eV as shown in Fig. S6 of the SM.[49] Therefore, the case of $U_{\text{eff}} \geq 3.0$ eV will be excluded in the following investigations. These results reveal that the electronic properties of VAs undergo relatively large modifications based on the values of U_{eff}. Moreover, the topological semimetal properties are sensitive to the states near the Fermi level, so we conduct a comprehensive comparison across various effective U values in the following.

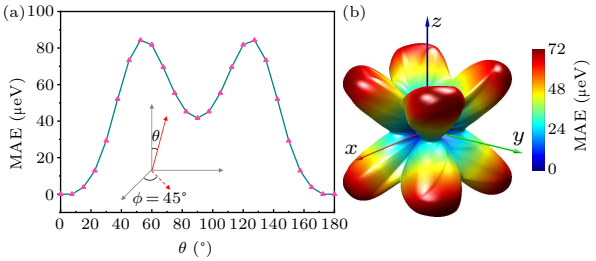


Fig. 3. The magnetic anisotropy energy of (a) $\phi = 45°$, and (b) the energy differences of VAs in the magnetization directions of different θ and ϕ.

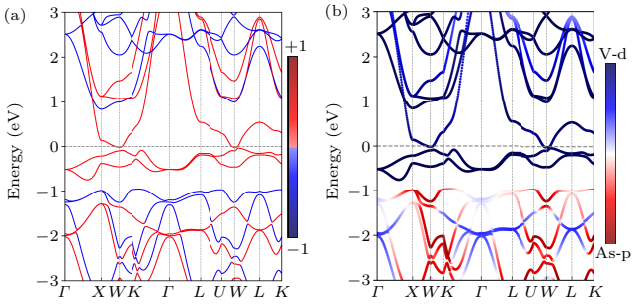


Fig. 4. (a) The spin projected band structures and (b) projected band structure of V-d orbitals and As-p orbitals of VAs using PBE functionals with considering SOC effect in the magnetization direction [001].

We start our exploration by investigating the electronic properties in the case of $U_{\text{eff}} = 1.5$ eV and the magnetization moment of V element is obtained to be $2.0\mu_{\text{B}}$ per unit formula. Moreover, the magnetic anisotropy energy (MAE), namely, $\text{MAE}_\theta = E_{[\theta]} - E_{[001]}$, is calculated and displayed in Fig. 3. Figure 3(b) suggests that the low-energy magnetic states are in the axis directions. As displayed in Fig. 3(a), we fix ϕ in 45° and change θ from 0° to 180° and find that the lowest magnetic order is along the [001] direction. Therefore, in the following, we will center on the magnetic direction of [001]. The band structures along high symmetry paths are plotted in Fig. 4 with the SOC effect. The first BZ and the high symmetry paths are marked by red arrows in Fig. S3. Figure 4(a) shows the spin-projected band structure, the red line represents the spin-up component and the blue lines represent the spin-down component. The spin-resolved band structure illustrates that the spin components are clearly separated because of the weak SOC interactions. The electronic contributions near the Fermi level are completely spin-up components, denoting the fully spin-polarized half-metallic features. Meanwhile, the projected electronic band structure of V-d and As-p orbitals of VAs is displayed in Fig. 4(b). It suggests that the main contribution around the Fermi level is V-d orbitals.

Now we focus on investigating the topological semimetallic properties of VAs. Figure S4(b) in the SM[49] shows the comparisons of the band structures obtained from PBE functionals and the MLWFs in consideration of the SOC effect. The fitting precision of MLWFs is in good agreement with the PBE results, suggesting the validation of the following calculations. The surface states and Fermi arcs for both (001) and (111) surfaces (Figs. 5 and 6) are obtained based on the Green function method.[52,53] Figures 5(a)–5(d) show the projected surface states and Fermi surfaces in the magnetic direction [001]. Figure 5(a) shows the projected surface states on the (001) surfaces, and the reciprocal high-symmetry points and paths of the projected surface are marked by white points and dotted lines in Fig. 5(b). By carefully checking the energy differences between the lowest conduction and the highest valence bands, we find that there are twelve pairs of WPs over the entire BZ. The coordinates of all twelve pairs of WPs are obtained and tabulated in Table 1. The coordinates of these WPs are asymmetrically distributed in the first BZ due to the lack of time-reversal and inversion symmetries. The energies of these WPs are very close to the Fermi energy, i.e., -0.073 eV, -0.025 eV, and 0.022 eV, respectively. Figures 5(b)–5(d) show the corresponding Fermi surfaces projected on the (001) surface of VAs. The Fermi arcs connected by opposite topological charges (± 1) of WPs (red for $+1$ and yellow for -1) are clearly visible among eight pairs of them while the Fermi arcs of the other four pairs of WPs (two pairs surrounded by cyan dotted circles and two pairs by yellow dotted circles) are covered by bulk states and can be visible in energies of 0.022 eV (Fig. 5(c)) and -0.073 eV (Fig. 5(d)), respectively. Meanwhile, the high energy magnetic order of magnetic direction [111] direction of VAs is also investigated and displayed in Fig. S5 of the SM.[49] As listed in Table S1, there still exist twelve pairs of WPs in the entire BZ and the energies and positions of these WPs are slightly different from the corresponding results in the magnetic direction [001]. These results reveal that the magnetic order can only move the WPs and does not eradicate these WPs, suggesting the robustness of these WPs. The WPs shown in Table S1 are even closer to the Fermi energy than previous results in Table 1. Meanwhile, the Fermi arcs of all the WPs in magnetic direction [111] can be clearly observed in the energies of 0.0 eV and -0.05 eV as displayed in Figs. S5(b) and S5(c). In addition, within the U_{eff} range of 1.5 eV to 2.5 eV, VAs consistently retain Weyl semimetal properties. Detailed results and corresponding figures can be found in Figs. S7–S10 and Tables S2–S3. Specifically, at $U_{\text{eff}} = 2.0$ eV, there still exist twelve pairs of Weyl points, and this number increases to fourteen pairs when U_{eff} is set at 2.5 eV.

Table 1. The corresponding positions, topological charges, and energies of the WPs in the magnetization direction [001] of VAs.

Coordinate (x, y, z)	Charge	$E - E_{\text{F}}$ (eV)
$(0.0, -1.0, -0.46)$	-1	0.022
$(-0.46, 0.0, -1.0)$	-1	-0.028
$(0.48, -1.0, 0.0)$	$+1$	-0.023
$(0.48, 0.0, 1.0)$	-1	-0.018
$(0.46, 0.0, -1.0)$	-1	-0.027
$(-0.48, 1.0, 0.0)$	$+1$	-0.023
$(0.0, -0.47, -1.0)$	$+1$	-0.018
$(1.0, 0.48, 0.0)$	-1	-0.023
$(-0.48, -1.0, 0.0)$	$+1$	-0.023
$(0.48, 1.0, 0.0)$	$+1$	-0.023
$(-0.48, 0.0, 1.0)$	-1	-0.018
$(1.0, 0.0, -0.50)$	$+1$	-0.073
$(0.0, 1.0, 0.5)$	-1	-0.074
$(-1.0, 0.0, -0.5)$	$+1$	-0.074
$(0.0, -1.0, 0.5)$	-1	-0.073
$(0.0, 0.45, 1.0)$	$+1$	-0.028
$(-1.0, -0.48, 0.0)$	-1	-0.023
$(-1.0, 0.48, 0.0)$	-1	-0.023
$(1.0, 0.0, 0.45)$	$+1$	0.022
$(1.0, -0.48, 0.0)$	-1	-0.022
$(0.0, 0.48, -1.0)$	$+1$	-0.018
$(-1.0, 0.0, 0.45)$	$+1$	0.022
$(0.0, 1.0, -0.45)$	-1	0.022
$(0.0, -0.46, 1.0)$	$+1$	-0.027

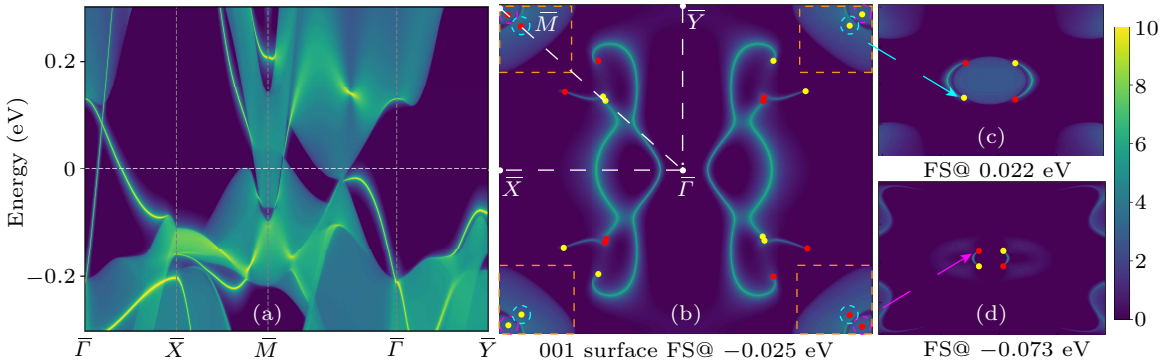


Fig. 5. Topological surface states and Fermi arcs projected on semi-infinite (001) surface. (a) The local density of states (LDOS) for (001) surface of VAs in the magnetic direction [001]. The paths for LDOS in panel (a) are marked with white dashed lines in panel (b). (b)–(d) The projected Fermi surface for VAs in magnetic direction [001] at three different energies of -0.025 eV, 0.022 eV, and -0.073 eV, respectively. The red and yellow dots represent the projections of WPs with the topological charge of $\mathcal{C} = 1$ and $\mathcal{C} = -1$, respectively.

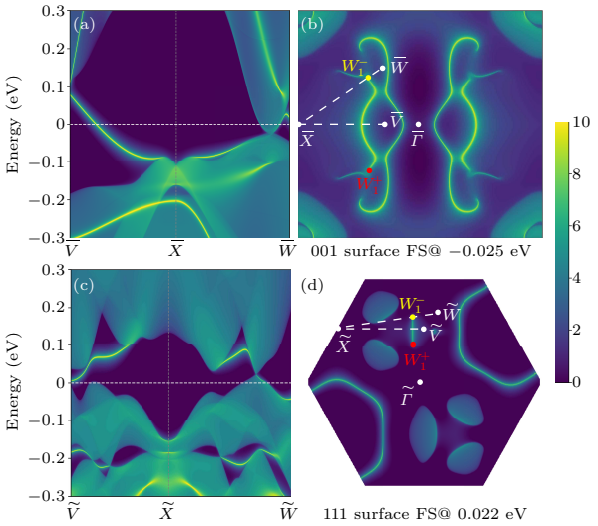


Fig. 6. Topological surface states and Fermi arcs projected on semi-infinite (001) and (111) surfaces. [(a) and (c)] The topological surface states for (001) and (111) surfaces of VAs in the magnetic direction [001], in which the high symmetry paths for the corresponding surface are marked by white dashed lines in panels (b) and (d). [(b) and (d)] The projected Fermi surfaces for VAs, in which the energies are marked at the bottom of the corresponding figures.

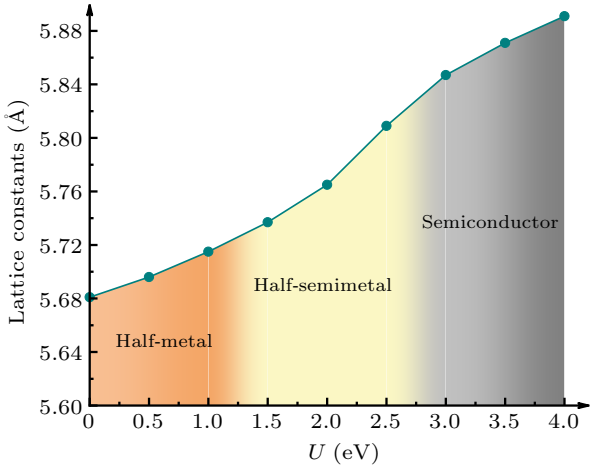


Fig. 7. Phase diagram and lattice constants versus U_{eff} values.

Next, in the case of $U_{\text{eff}} = 1.5$ eV, we select two energies (i.e., -0.025 eV and 0.022 eV) with respect to the Fermi energy to clearly show the topological surface states. Figures 6(a)–6(d) show the results of the surface states and Fermi surfaces which are projected on (001) and (111) surfaces. The corresponding high symmetry paths are marked by white dashed lines in Figs. 6(b) and 6(d), respectively. In (001) surface, the Weyl cone along $\overline{X}$–$\overline{W}$ is clearly visible, and the surface states connect the valance band and the conduction band. The projected Fermi arcs in Fig. 6(b) along $\overline{V}$–$\overline{X}$ can also be visible in Fig. 6(a). The projected surface states and Fermi arcs on the (111) surface in Figs. 6(c) and 6(d) also give clear results. These results demonstrate that VAs is a Weyl semimetal. Combined with the half-metal features of VAs, it can be concluded that VAs is a fully spin-polarized semimetal ferromagnet. As the energies of WPs are very close to the Fermi level, it will be better for direct experimental observations. We meticulously examine electronic properties by systematically scanning U_{eff} values within the range of 0 eV to 2.5 eV, with an energy spacing of 0.5 eV, and plot the phase diagram in Fig. 7. The lattice constants undergo a measured expansion as U values vary, leading to subtle shifts in electronic behavior. Notably, discernible topological phase transitions manifest which stems from the intricate interplay of correlation effects. To provide unequivocal evidence of the Weyl semimetal properties inherent in VAs, we have further scrutinized the crossing points by systematically scanning these Weyl points (WPs) within the DFT + DMFT regime. Figure S11 shows the conspicuous cross features observed in the DFT + DMFT band structures, specifically in the spin-up component. These findings strongly indicate that VAs is a half-Weyl semimetal, and can be described by DFT + U methods with effective U values falling within the 1.5 eV to 2.5 eV range.

In summary, based on DFT and DMFT theory, we investigate the half-metallic ferromagnet VAs which is confirmed to be a half-metallic ferromagnet with dynamic correlations. Using the DFT + DMFT as a reference benchmark, we investigate the electronic properties of VAs within the DFT + U regime. As the states near the Fermi level are sensitive to the U_{eff} values, we systematically explore its electronic properties by scanning the U_{eff} values from 0 eV to 4.0 eV. In the U_{eff} range of 0 eV–1.0 eV, VAs exhibits trivial half-metal properties, while revealing nontrivial Weyl semimetal properties within the 1.5 eV–2.5 eV range. Taking $U_{\text{eff}} = 1.5$ eV as an example, and considering the SOC effect, the magnetic anisotropic energy of VAs suggests a potential ground state with magnetic orders along the [001] directions. The magnetic moment is obtained to be $2\mu_{\text{B}}$ for the V element per unit formula. We further delve into the topological aspects, investigating surface states and Fermi arcs projected on semi-infinite (001) and (111) surfaces. Notably, the change in magnetic direction only affects the positions of Weyl points. Both in the magnetic directions [001] and [111], twelve pairs of Weyl points with opposite topological charges (+1 and −1) span the entire Brillouin zone. The Fermi arcs of all Weyl points are observable across different energies and surfaces, solidifying the magnetic topological Weyl semimetal properties of VAs. The crossing features of the DFT + DMFT band structure also support the Weyl characteristics of VAs. These results suggest the fully spin-polarized Weyl semimetal characteristics observed in VAs compound and present compelling prospects for advancing fundamental research in many-body physics and spintronics.

Acknowledgments

Project supported by the National Natural Science Foundation of China (Grant Nos. 12204074, 12222402, 92365101,

and 12347101) and the Natural Science Foundation of Chongging (Grant No. CSTB2023NSCQ-JQX0024).

References

[1] De Groot R, Mueller F, van Engen P V and Buschow K 1983 *Phys. Rev. Lett.* **50** 2024
[2] De Groot R, Mueller F, Van Engen P and Buschow K 1984 *J. Appl. Phys.* **55** 2151
[3] De Groot R and Buschow K 1986 *J. Magn. Magn. Mater.* **54** 1377
[4] Benmakhlouf A, Bourourou Y, Bouhemadou A, Bentabet A, Khemloul F, Maabed S, Bouchenafa M and Galanakis I 2018 *J. Magn. Magn. Mater.* **465** 430
[5] Şaşioglu E, Galanakis I, Sandratskii L M and Bruno P 2005 *J. Phys. Condens. Matter.* **17** 3915
[6] Irkhin V Y and Katsnel'son M I 1994 *Phys. Usp.* **37** 659
[7] Žutić I, Fabian J and Das Sarma S 2004 *Rev. Mod. Phys.* **76** 323
[8] Chappert C, Fert A and Van Dau F N 2007 *Nat. Mater.* **6** 813
[9] Soulen Jr R, Byers J, Osofsky M, Nadgorny B, Ambrose T, Cheng S, Broussard P R, Tanaka C, Nowak J, Moodera J, *et al.* 1998 *Science* **282** 85
[10] Korotin M, Anisimov V, Khomskii D and Sawatzky G 1998 *Phys. Rev. Lett.* **80** 4305
[11] Yanase A and Siratori K 1984 *J. Phys. Soc. Jpn.* **53** 312
[12] Galanakis I, Dederichs P and Papanikolaou N 2002 *Phys. Rev. B* **66** 134428
[13] Galanakis I, Dederichs P and Papanikolaou N 2002 *Phys. Rev. B* **66** 174429
[14] Galanakis I 2004 *J. Phys. Condens. Matter.* **16** 3089
[15] Shreder E, Streltsov S, Svyazhin A, Makhnev A, Marchenkov V, Lukoyanov A and Weber H 2008 *J. Phys. Condens. Matter.* **20** 045212
[16] Fomina K, Marchenkov V, Shreder E and Weber H 2011 *Solid State Phenom.* **168** 545
[17] Shreder E, Makhnev A, Lukoyanov A and Suresh K 2017 *Phys. Met. Metallogr.* **118** 965
[18] Lidig C, Minár J, Braun J, Ebert H, Gloskovskii A, Krieger J A, Strocov V, Kläui M and Jourdan M 2019 *Phys. Rev. B* **99** 174432
[19] Jourdan M, Minár J, Braun J, Kronenberg A, Chadov S, Balke B, Gloskovskii A, Kolbe M, Elmers H J, Schönhense G, *et al.* 2014 *Nat. Commun.* **5** 3974
[20] Akai H 1998 *Phys. Rev. Lett.* **81** 3002
[21] Sandratskii L and Bruno P 2002 *Phys. Rev. B* **66** 134435
[22] Wang X L 2008 *Phys. Rev. Lett.* **100** 156404
[23] Ouardi S, Fecher G H, Felser C and Kübler J 2013 *Phys. Rev. Lett.* **110** 100401
[24] Manna K, Sun Y, Muechler L, Kübler J and Felser C 2018 *Nat. Rev. Mater.* **3** 244
[25] Wang X L 2017 *Natl. Sci. Rev.* **4** 252
[26] Cheng X, Xu S, Jia F, Zhao G, Hu M, Wu W and Ren W 2021 *Phys. Rev. B* **104** 104417
[27] Mogulkoc A, Modarresi M and Rudenko A N 2020 *Phys. Rev. B* **102** 024441
[28] Hedin L 1965 *Phys. Rev.* **139** A796
[29] Damewood L and Fong C Y 2011 *Phys. Rev. B* **83** 113102
[30] Gao R, Liu C, Fang L, Yao B, Wu W, Xiao Q, Hu S, Liu Y, Gao H, Cao S, *et al.* 2022 *Chin. Phys. Lett.* **39** 127301
[31] Xiang W, Wang Y, Ji W, Hou W, Li S and Wang P 2023 *Chin. Phys. B* **32** 037103
[32] Galanakis I and Mavropoulos P 2003 *Phys. Rev. B* **67** 104417
[33] Akinaga H, Manago T and Shirai M 2000 *Jpn. J. Appl. Phys.* **39** L1118
[34] Shirai M 2003 *J. Appl. Phys.* **93** 6844
[35] Dong X, Jia X, Yan Z, Shen X, Li Z, Qiao Z and Xu X 2023 *Chin. Phys. Lett.* **40** 087301
[36] Sanyal B, Bergqvist L and Eriksson O 2003 *Phys. Rev. B* **68** 054417
[37] Chioncel L, Mavropoulos P, Ležaić M, Blügel S, Arrigoni E, Katsnelson M I and Lichtenstein A I 2006 *Phys. Rev. Lett.* **96** 197203
[38] Wan X, Turner A M, Vishwanath A and Savrasov S Y 2011 *Phys. Rev. B* **83** 205101
[39] Xu G, Weng H, Wang Z, Dai X and Fang Z 2011 *Phys. Rev. Lett.* **107** 186806
[40] Lv B, Weng H, Fu B, Wang X P, Miao H, Ma J, Richard P, Huang X, Zhao L, Chen G, *et al.* 2015 *Phys. Rev. X* **5** 031013
[41] Lu L, Wang Z, Ye D, Ran L, Fu L, Joannopoulos J D and Soljačić M 2015 *Science* **349** 622
[42] Xu S Y, Alidoust N, Belopolski I, Yuan Z, Bian G, Chang T R, Zheng H, Strocov V N, Sanchez D S, Chang G, *et al.* 2015 *Nat. Phys.* **11** 748
[43] Borisenko S, Evtushinsky D, Gibson Q, Yaresko A, Koepernik K, Kim T, Ali M, van den Brink J, Hoesch M, Fedorov A, *et al.* 2019 *Nat. Commun.* **10** 3424
[44] Weng H, Fang C, Fang Z, Bernevig B A and Dai X 2015 *Phys. Rev. X* **5** 011029
[45] Wang Z, Vergniory M, Kushwaha S, Hirschberger M, Chulkov E, Ernst A, Ong N P, Cava R J and Bernevig B A 2016 *Phys. Rev. Lett.* **117** 236401
[46] Nie S, Hashimoto T and Prinz F B 2022 *Phys. Rev. Lett.* **128** 176401
[47] Marzari N, Mostofi A A, Yates J R, Souza I and Vanderbilt D 2012 *Rev. Mod. Phys.* **84** 1419
[48] Mostofi A A, Yates J R, Pizzi G, Lee Y S, Souza I, Vanderbilt D and Marzari N 2014 *Comput. Phys. Commun.* **185** 2309
[49] See supplementary material for the theoretical background of DFT + DMFT methods, the calculations details, list of the positions of WPs, topological surface states and Fermi arcs, etc., which include Refs. [47,48,54–65].
[50] Gull E, Millis A J, Lichtenstein A I, Rubtsov A N, Troyer M and Werner P 2011 *Rev. Mod. Phys.* **83** 349
[51] Haule K 2007 *Phys. Rev. B* **75** 155113
[52] Yu R, Wu Q, Fang Z and Weng H 2017 *Phys. Rev. Lett.* **119** 036401
[53] Sancho M P L, Sancho J M L and Rubio J 1984 *J. Phys. F: Met. Phys.* **14** 1205
[54] Singh V, Herath U, Wah B, Liao X, Romero A H and Park H 2021 *Comput. Phys. Commun.* **261** 107778
[55] Savrasov S Y and Kotliar G 2004 *Phys. Rev. B* **69** 245101
[56] Kotliar G, Savrasov S Y, Haule K, Oudovenko V S, Parcollet O and Marianetti C A 2006 *Rev. Mod. Phys.* **78** 865
[57] Jarrell M 1992 *Phys. Rev. Lett.* **69** 168
[58] Shinaoka H, Assaad F, Blümer N and Werner P 2017 *Eur. Phys. J. Spec. Top.* **226** 2499
[59] Kohn W and Luttinger J M 1960 *Phys. Rev.* **118** 41
[60] Luttinger J M and Ward J C 1960 *Phys. Rev.* **118** 1417
[61] Luttinger J M 1961 *Phys. Rev.* **121** 942
[62] Kresse G and Furthmüller J 1996 *Phys. Rev. B* **54** 11169
[63] Kresse G and Furthmüller J 1996 *Comput. Mater. Sci.* **6** 15
[64] Perdew J P, Burke K and Ernzerhof M 1996 *Phys. Rev. Lett.* **77** 3865
[65] Li W, Carrete J, Katcho N A and Mingo N 2014 *Comput. Phys. Commun.* **185** 1747